



HAL
open science

Donor-Acceptor Pairs Recombination as the Origin of the Emission Shift In InGaN/GaN Scintillator Heterostructures Doped with Zn

František Hájek, Vítězslav Jarý, Tomáš Hubáček, Filip Dominec, Alice Hospodková, Karla Kuldová, Jiří Oswald, Jiří Pangrác, Tomáš Vaněk, Maksym Buryi, et al.

► **To cite this version:**

František Hájek, Vítězslav Jarý, Tomáš Hubáček, Filip Dominec, Alice Hospodková, et al.. Donor-Acceptor Pairs Recombination as the Origin of the Emission Shift In InGaN/GaN Scintillator Heterostructures Doped with Zn. *ECS Journal of Solid State Science and Technology*, 2023, 12 (6), pp.066004. 10.1149/2162-8777/acda62 . hal-04156893

HAL Id: hal-04156893

<https://hal.science/hal-04156893>

Submitted on 20 Nov 2023

HAL is a multi-disciplinary open access archive for the deposit and dissemination of scientific research documents, whether they are published or not. The documents may come from teaching and research institutions in France or abroad, or from public or private research centers.

L'archive ouverte pluridisciplinaire **HAL**, est destinée au dépôt et à la diffusion de documents scientifiques de niveau recherche, publiés ou non, émanant des établissements d'enseignement et de recherche français ou étrangers, des laboratoires publics ou privés.

OPEN ACCESS

Donor-Acceptor Pairs Recombination as the Origin of the Emission Shift In InGaN/GaN Scintillator Heterostructures Doped with Zn

To cite this article: František Hájek *et al* 2023 *ECS J. Solid State Sci. Technol.* **12** 066004

View the [article online](#) for updates and enhancements.

You may also like

- [Review—Recent Advances and Challenges in Indium Gallium Nitride \(In_xGa_{1-x}N\) Materials for Solid State Lighting](#)
Ravinder Kour, Sandeep Arya, Sonali Verma *et al.*
- [Recent progress in red light-emitting diodes by III-nitride materials](#)
Daisuke Iida and Kazuhiro Ohkawa
- [Review—The Physics of Recombinations in III-Nitride Emitters](#)
Aurelien David, Nathan G. Young, Cory Lund *et al.*



245th ECS Meeting • May 26-30, 2024 • San Francisco, CA

Present your work at the leading electrochemistry & solid-state science conference.

Network with academic, government, and industry influencers!

Submit abstracts by December 1, 2023

[Learn more & submit!](#)





Donor-Acceptor Pairs Recombination as the Origin of the Emission Shift In InGaN/GaN Scintillator Heterostructures Doped with Zn

František Hájek,^{1,2,z} Vítězslav Jarý,¹ Tomáš Hubáček,¹ Filip Dominec,¹ Alice Hospodková,¹ Karla Kuldová,¹ Jiří Oswald,¹ Jiří Pangrác,¹ Tomáš Vaněk,¹ Maksym Buryi,¹ Gilles Ledoux,³ and Christophe Dujardin³

¹Institute of Physics of the Czech Academy of Sciences, Prague 6, Czech Republic

²Czech Technical University in Prague, Faculty of Nuclear Sciences and Physical Engineering, Prague 1, Czech Republic

³Institut Lumière Matière, UMR55306 Université Claude Bernard, Lyon 1-CNRS, France

We report luminescence decay characteristics of the InGaN/GaN scintillator heterostructures doped with Zn. Unusually large shifting of luminescence band caused by Zn acceptors incorporated in InGaN is observed both in time-resolved and excitation-dependent spectra. Origins of the shifts are discussed, and model based on donor-acceptor pair recombination is introduced. The results imply a shrinkage of donor Bohr radius compared to the bulk material caused by quantum confinement effect. The slow decay of Zn band points out to the necessity of Zn impurity elimination in applications requiring fast timing characteristics of a scintillator.

© 2023 The Author(s). Published on behalf of The Electrochemical Society by IOP Publishing Limited [DOI: 10.1149/2162-8777/acda62]

This article was made open access on 31 July and may be distributed under the terms of the Creative Commons Attribution-Non Commercial-No Derivatives 4.0 License (CC BY-NC-ND 4.0, <http://creativecommons.org/licenses/by-nc-nd/4.0/>), which permits restricted non-commercial reuse of the work in any medium provided the original work is properly cited.



Manuscript submitted April 20, 2023; revised manuscript received May 19, 2023. Published June 19, 2023. *This paper is part of the JSS Focus Issue on Recent Developments in Theory, Measurements and Applications of Luminescent Materials: A Tribute to Prof. B. Di Bartolo.*

A large demand for scintillators with fast response leads to investigating new materials from the perspective of high-energy radiation response. InGaN/GaN heterostructures with decay times in order of ns are one of the promising candidates in applications like Time-of-Flight Positron Emission Tomography (TOF-PET).^{1–3} One of their advantage is the quantum confinement of excited carriers in few nanometers thick InGaN layer acting as a potential well since InGaN bandgap is lower than GaN. The carriers excited in structure (mainly in GaN layers) are redistributed on ps time scale after excitation to the InGaN quantum well (QW) and the local concentration of carriers is therefore higher than in bulk material, making the influence of non-radiative centers less pronounced. This makes the radiative recombination in InGaN QWs highly efficient. Moreover, the emission energy from InGaN QWs is lower than the GaN bandgap, meaning that the self-absorption effect is negligible. However, several issues concerning InGaN/GaN scintillators must be solved: except problems arising from limited thickness of InGaN/GaN active region, the unwanted defect luminescence with long decay times is a significant obstacle hindering the widespread of nitride-based materials as scintillators. Therefore, understanding the defect nature and their recombination mechanisms is of great importance nowadays.

Zinc impurities are one of the common contaminants found in GaN and InGaN layers grown by Metal Organic Vapour Phase Epitaxy (MOVPE). Their behavior is quite well-documented since Zn doping of InGaN was studied as a potential solution for fabrication of white light-emitting diodes (LEDs).^{4–6} The Zn doping results into broad luminescence band (ZnB) shifted about 400–500 meV to lower energies than the main luminescence peak originating from InGaN band-to-band recombination. The origin of ZnB was assigned to donor-acceptor pair (DAP) recombination between Si donors and Zn acceptors.^{4,5} In GaN, Zn forms a relatively deep acceptor when substituting Ga atom with the energy level around 390 meV from the valence band⁷ while Si acts as a shallow donor with ionization energy of 25 meV when introduced in low concentration.⁸ However, there is a lack of reports considering the luminescence decay kinetics of ZnB in literature despite the decay kinetics is important factor for scintillator development.

ZnB exhibit unusually large spectral blue-shifting with increasing excitation intensity. Several explanations of the shifts were provided

by different authors. They were assigned to tunnelling currents,⁹ band filling effect alongside with piezoelectric field screening,¹⁰ competition between different luminescence bands⁶ and the DAP recombination mechanism. In the latter case the shift happens due to the Coulombic interaction between ionized donors and acceptors.⁵ The large shifts were actually one of the reasons why the InGaN:(Zn, Si) failed on the white LED market.

In this paper, steady-state, and time-resolved Photoluminescence (PL) and Secondary ion mass spectroscopy (SIMS) measurements are applied to study the luminescence decay of ZnB and to resolve the origin of ZnB luminescence shifts. A phenomenological model is used to explain the large shifts by DAP recombination involving donor with lowered Bohr radius due to the quantum confinement in InGaN layers.

Experimental

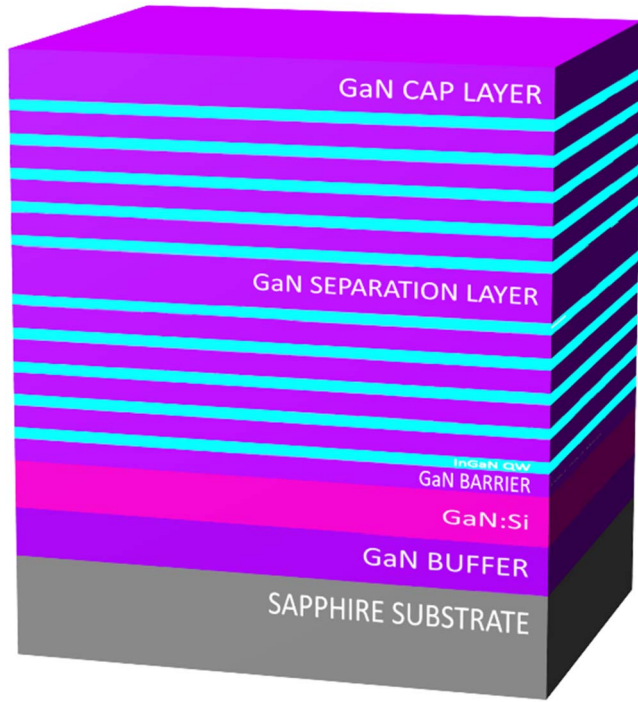
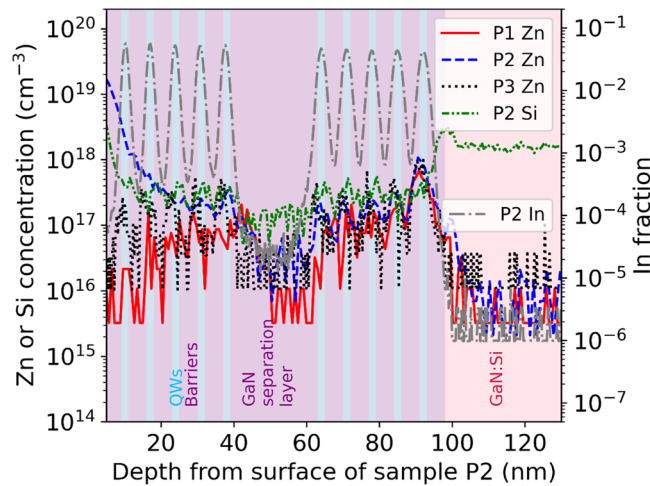
Samples were prepared by MOVPE on a *c*-oriented sapphire substrate. First, commonly applied GaN buffer layer was deposited. More information can be found in Ref. 11. Trimethylgallium was used as Ga precursor and NH₃ as the nitrogen one. These layers were grown in H₂ atmosphere. Then, Si-doped GaN was grown (Si doping was employed to smear the piezoelectric field inside the QWs and thus increase the electron-hole wavefunction overlap). A thin low-temperature (LT) GaN was placed between GaN buffer and InGaN/GaN active region to incorporate impurities flowing on the growth surface.¹² InGaN/GaN active region was grown from Triethylgallium precursor for Ga, Trimethylindium for In and NH₃ for nitrogen in N₂ atmosphere. More information can be found in Ref. 13. The first 5 InGaN QWs separated by GaN barriers were grown followed by GaN separation layer and another stack of 5 QWs and barriers. Average In concentration in InGaN QW was 5% and the QW thickness was 1.6 nm. The Zn doping in InGaN QWs is not intentional and varies among the samples. The samples P1, P2 and P3 studied in this work are nominally identical except the growth parameters listed in Table I. The whole structure is capped by thin GaN layer. The structure is schematically shown in Fig. 1. Please note that InGaN QWs are also doped by Si (shallow donor¹⁴) which diffuses from the GaN:Si layer, see Fig. 2. The Si doping is utilized to screen the electric fields in the quantum well region which originate from the difference in spontaneous and piezoelectric field polarizations between GaN and InGaN.

Steady-state photoluminescence was measured with confocal microscope LabRAM HR Evolution with He-Cd laser (excitation

^zE-mail: hajek@fzu.cz

Table I. Growth parameters of the studied samples.

Sample	GaN cap thickness (nm)	Si nominal concentration in buffer [cm^{-3}]	LT GaN thickness [nm]
P1	65	1×10^{18}	8
P2	12	3×10^{18}	60
P3	12	1×10^{18}	8

**Figure 1.** Schematic drawing of the sample structure (not to scale).**Figure 2.** SIMS measurement of samples P1, P2 and P3. Signal of sample P1 is shifted because of the thicker cap layer atop the structure.

wavelength 325 nm) and UV-compatible objective CG74. The spot diameter was $2 \mu\text{m}$ and the penetration depth of the excitation light was around 100 nm (absorption coefficient $1.2 \times 10^4 \text{ cm}^{-1}$).¹⁵

PL decay curves were measured by a custom-made spectrofluorometer 5000 M (Horiba Jobin Yvon, Wildwood, MA, USA) using nanosecond nanoLED pulsed light sources in time-correlated single-photon counting mode (Horiba Scientific) as the excitation sources. The detection part of the setup involved a single-grating

monochromator and a photon-counting detector TBX-04 (Hamamatsu). Measured spectra were corrected for the spectral dependence of detection sensitivity.

Time-resolved radioluminescence was measured with soft X-ray pulses generated by a picosecond pulsed laser from Hamamatsu (illuminating the photocathode of X-ray tube) with pulse duration of 51 ps and the detected emission was set at 379 nm. Detection was done by a PMA 182 photomultiplier from PicoQuant connected to a PicoHarp 300 multichannel analyzer. We also used 10 nm bandpass filters centered at 379 nm to obtain response only from the excitonic band.

The photoluminescence-excitation spectra in the form of 2D contour plots of prepared samples were measured on a custom apparatus. The sample was illuminated by a EQ99X laser driven light source filtered by a Gemini 180 monochromator (Jobin Yvon). The light from the monochromator exit slit was then focused on the sample by two 2-inch-diameter MgF_2 lenses with a focal length of 100 mm. The whole apparatus has been calibrated by means of a Newport 918D Low power calibrated photodiode sensor over the range 190–1000 nm, the resolution of the system being 4 nm. The emitted light from the sample was collected by an optical fiber connected to a TRIAX320 monochromator (Jobin Yvon) equipped with a cooled CCD detector. At the entrance of the monochromator, different long pass filters were chosen in order to eliminate the excitation light. The spectral resolution of the detection system was 2 nm. Excitation intensity is in order of $10^{-4} \text{ W cm}^{-2}$ in the spectral region of interest. All emission spectra were transformed from nm to eV scale using Jacobian transformation. Since the excitation spectra are calibrated by a photodiode, no correction is needed when transformation to eV scale takes place.¹⁶

Secondary ion mass spectroscopy measurements were performed by EAG laboratories.

Results

Concentration quenching of Zn in GaN was reported at concentrations about $8 \cdot 10^{18} \text{ cm}^{-3}$,¹⁷ which is far beyond the usual unintentional doping level. The ZnB photoluminescence intensity is thus expected to be proportional to Zn concentration. To reveal relationship between Zn band in PL and Zn concentration in samples, SIMS measurements were performed on three samples P1, P2 and P3. Figure 2 shows the SIMS profile of Zn for all samples in the vicinity of the quantum well region, the origin of x axis is at the surface of sample P2 and P3. Sample P1 has thicker capping layer so the SIMS profile of sample P1 is shifted by the thickness of the capping layer for clarity to match the QW region of P1 on the one of sample P2 and P3. The grey dash-dot line represents the In signal from sample P2 and hence, marks positions of QWs. All samples show increased Zn concentration by almost 1 order of magnitude in InGaN QWs compared to GaN barriers. SIMS signal is disturbed by the surface artefacts for the top 5 QWs in the case of sample P2. Si concentration for sample P2 is also shown in Fig. 2. Preferential incorporation of residual Si into InGaN layers is observed (Fig. 2).

Photoluminescence spectra excited by 325 nm are shown in Fig. 3. Emission from InGaN quantum wells (QW) is observed at higher energy while the broad band at lower energy is assigned to the ZnB band. Both peaks were fitted with functions adapted to the origin of the bands. For QW recombination, the pseudo-Voigt function was used while the Zn bands were fitted with the model from,¹⁸ which takes into account the phonon interaction of a given

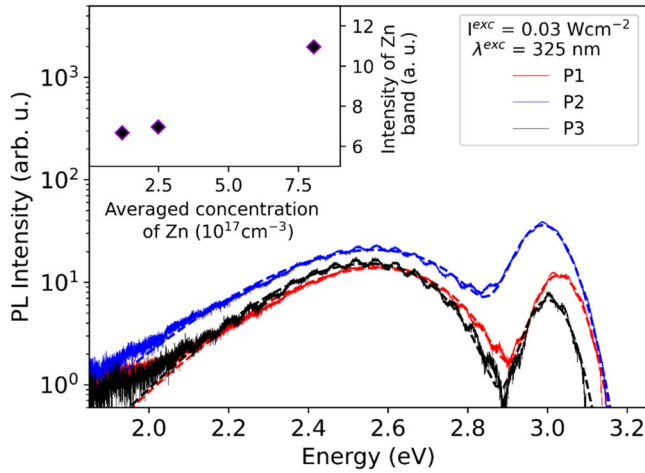


Figure 3. PL spectra of the samples P1, P2, and P3. Spectra were fitted (dashed lines) as described in the text. Inset shows the monotonic dependence of ZnB intensity on averaged Zn concentration in the InGaN layers.

luminescence centre with lattice:

$$I(h\nu) = I_{\max} \exp \left[-2S \left(\sqrt{\frac{E_0 - h\nu}{E_0 - h\nu_{\max}}} - 1 \right)^2 \right] \quad [1]$$

The intensity of ZnB is plotted against the averaged Zn concentration in the QWs measured by SIMS in inset of Fig. 3 (only data from the 5 QWs closer to the substrate were used because of the SIMS surface artefact of measurement). Monotonous dependence is observed suggesting that concentration quenching does not take place. So-called yellow luminescence commonly observed in GaN samples was almost more than two orders of magnitude weaker in our InGaN/GaN samples under laser 325 nm excitation conditions, so it was not included into the fitting procedure (checked on reference sample without InGaN QWs). Oscillations modifying the PL spectra are interference fringes and their period is determined by total thickness of nitride layers.

Excitation-emission map is shown in Fig. 4 for sample P1. Zn acceptors are known to have exceptionally large hole capture cross-section coefficients ($5 \times 10^{-7} \text{ cm}^3 \text{ s}^{-118}$) making them very effective luminescence centers and they can be the dominant recombination channel, especially at low excitation intensities before all Zn acceptors are saturated. Below GaN bandgap, absorption of excitation light is very weak (only in QWs) which leads to only observable band being ZnB. Under 3.38 eV (=366 nm) excitation energy, yellow band (YB) at 2.2 eV from carbon impurities which are present in GaN buffer¹⁹⁻²¹ emerges, too. The YB is not observed with the above bandgap excitation because in such case, the excitation light is absorbed in the QW region. On the other hand, YB is not observed for wavelengths much longer than GaN bandgap since the excitation of YB happens through shallow below-bandgap states of GaN. The problem of YB luminescence decay kinetics was described earlier in Ref. 22. In Ref. 22 we showed that the mean decay time of YB can be accelerated from millisecond range to hundreds of ns by Si or Ge doping of GaN buffer layer. Therefore, we found a way how to alter YB behavior not to be detrimental for scintillator application.

For the above GaN bandgap excitation wavelengths, ZnB alongside with QW emission are seen.

The temporal performance of a scintillator was tested by soft X-ray excitation. Beside the very fast component from QW luminescence (main component with characteristic decay time 0.4 ns), a component with very long decay time can be observed (Fig. 5) when no spectral filter is used. However, this component

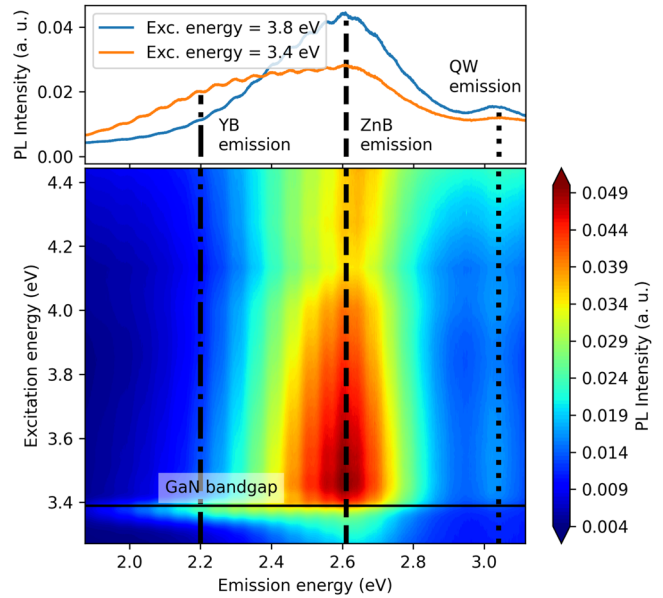


Figure 4. RT Excitation-emission map of sample P1. QW emission at 3.03 eV (dotted line) and ZnB emission at 2.61 eV (dashed line) are clearly observed for all excitation energies above the GaN bandgap. ZnB is observed also below GaN bandgap (3.39 eV, solid line). At 366 nm excitation, yellow band at 2.2 eV (dash-dot line) is observed. TOP: an emission spectrum from the map at excitation energies 3.8 eV (=325 nm) and 3.39 eV (=366 nm).

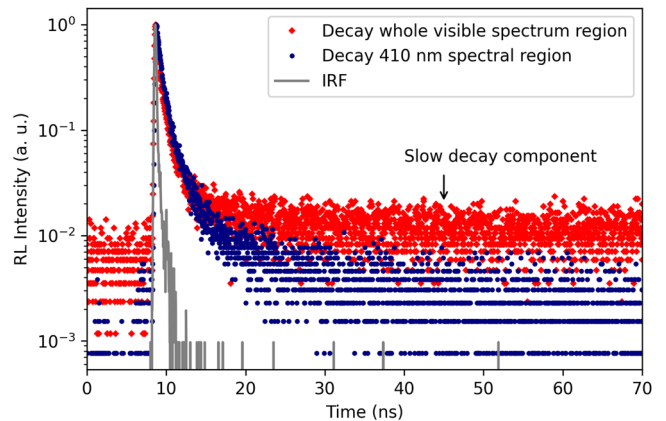


Figure 5. Time decay of luminescence excited by soft X-ray (sample P1). The whole visible spectral region measured (red), and with a filter centered at 410 nm (dark blue). Instrument response function (IRF) is also plotted (grey).

disappears when only QW emission is measured (filtered at 410 nm). Since the most pronounced spectral component aside from QW luminescence is ZnB (Figs. 3, 4), we ascribe this long component to this band. It should be noticed that this slow component was observed in our earlier study¹ and was incorrectly ascribed to yellow band coming from carbon on nitrogen site in GaN.^{23,24} In the following, we show by time-resolved photoluminescence that ZnB is responsible for this slow component.

The photoluminescence decays ZnB are non-exponential and wavelength-dependent. Therefore, time resolved spectra are convenient to understand the recombination mechanism. Time decays obtained for wavelengths with step 5 nm in the range 420–600 nm were divided into 20 time windows ranging from a few tens of ns to a few tens of microseconds. Time-resolved spectra were constructed from these time decay curves. Example of the time evolution of the spectra for sample P3 is shown in Fig. 6a (only 7 spectra are shown for better clarity). The ZnB shift towards lower energies at longer

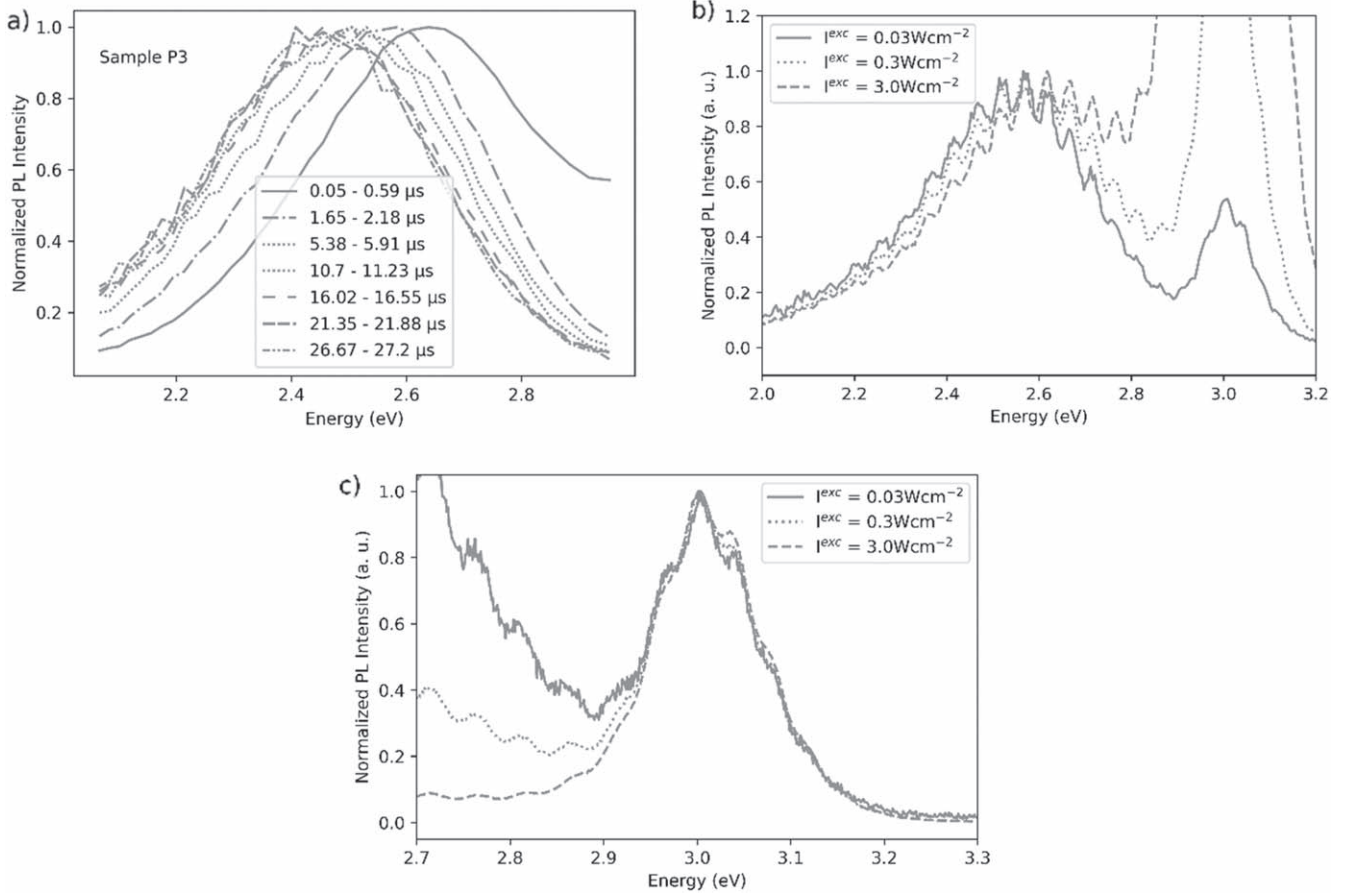


Figure 6. (a) Shift of the time-resolved PL spectra of sample P3. (b) shift of the steady-state spectra normalized to ZnB maximum of sample P3 with excitation intensity. Shift to the lower energies is clearly observed either with longer decay times or lower excitation intensities. (c) PL spectra normalized to QW peak maximum. No shift of QW peak is observed with different excitation intensities.

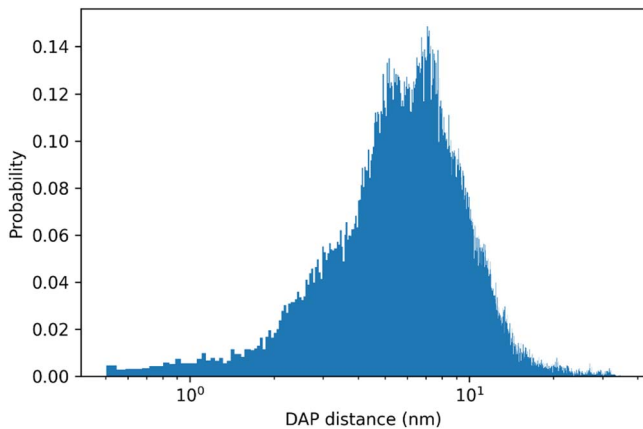


Figure 7. Distribution of donor acceptor pair distances in sample P3.

times can be clearly observed. Similarly, the shift of the ZnB is also seen with decreasing excitation intensity in steady state conditions (example of sample P3 is presented in Fig. 6b).

Several mechanisms could be hypothetically causing the observed shifting:

- 1) Competition of different channels. Since the shape of the band remains almost identical during the time evolution of the spectra or the change of excitation intensity, we rule out the possibility that the competition of different channels could be the main source of the band shift, as suggested in Ref. 17.

- 2) Tunneling currents. The tunneling currents as the origin of ZnB shifting⁹ can be excluded in our case since the excitation is not an electrical, but an optical one.
- 3) Electrical field in InGaN QWs. The influence of the electrical field caused by the difference in spontaneous and piezoelectric polarizations between InGaN and GaN should be considered as the cause for the band shift. If this field can be efficiently screened by excited charge, the shift happens both in time resolved-spectra and in excitation intensity-dependent PL spectra. However, this would also result in the shift of QW recombination peak, which is not observed (Fig. 6c).
- 4) Ion interaction with electric field. We could argue, that the shift of ZnB is caused by interaction of the Zn⁻ ions (which remain in the electric field after the recombination) with the polarization charge. But if we consider the magnitude of the effect, we have to reject this hypothesis: the polarization field in QWs is caused by interface charge in order of 10⁵ e μm⁻².²⁵ The number of Zn ions in the 2 nm wide QW and concentration 10¹⁸ cm⁻³ (upper limit in our samples measured by SIMS), is at least two orders of magnitudes smaller than the interface charge. Therefore, screening of the interface charge cannot lead to significant shift of the ZnB.
- 5) DAP recombination. Ruling out the foregoing sources of shifting, we will reflect on the possibility of DAP recombination being the source of the blueshift and introduce a model describing the energy shift during the time decay of DAP recombination.

In the DAP mechanism, the probability of recombination of one is given by²⁶

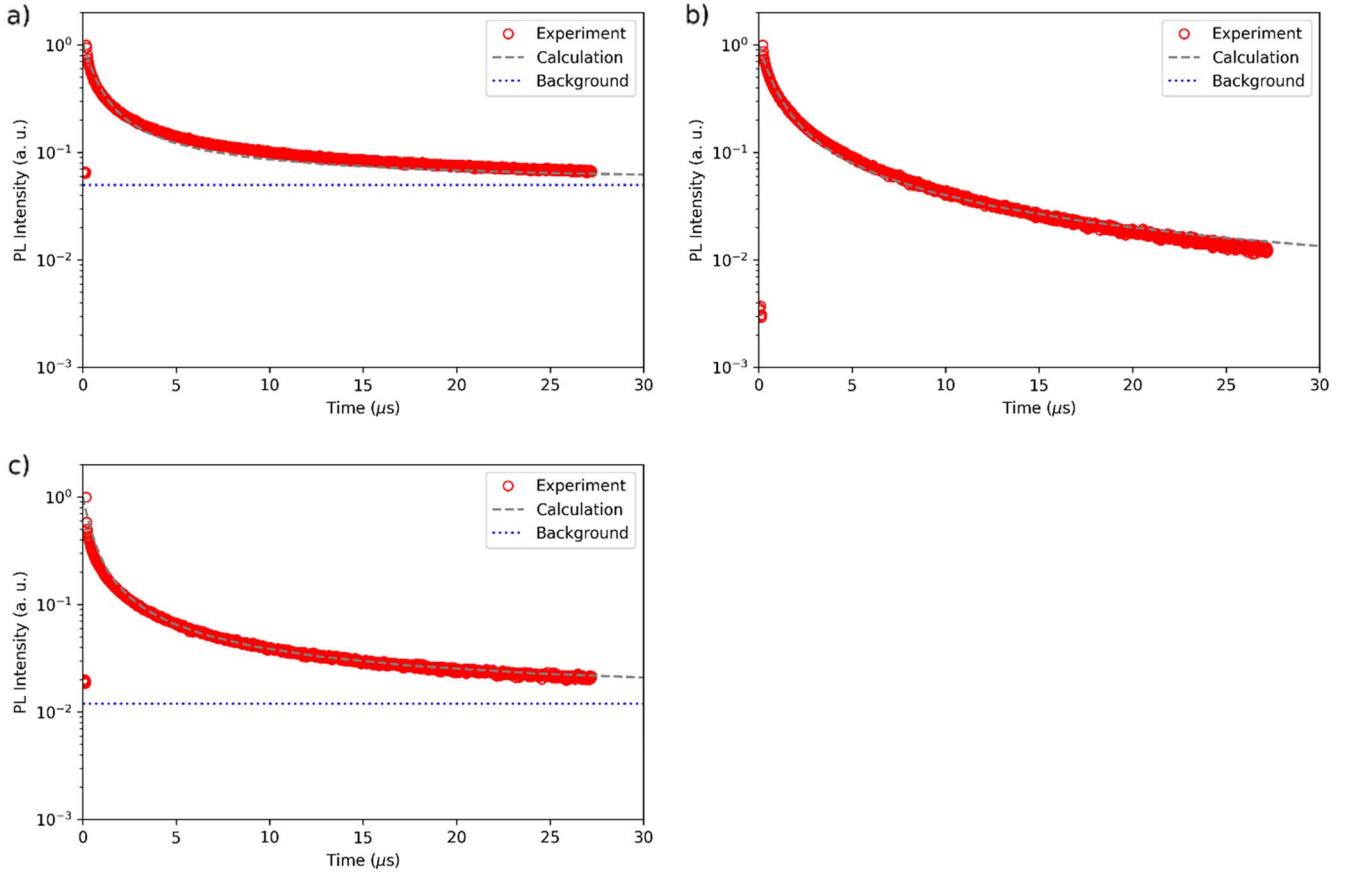


Figure 8. Decay curves of photoluminescence of ZnB for samples (a) P1, (b) P2, (c) P3 and the calculated curves using Eq. 4 and $G(R)$ from SIMS.

$$\frac{1}{\tau_{DAP}} = W(R) = W_0 \cdot e^{-\frac{2R}{a_D}} \quad [2]$$

The a_D is the Bohr radius of the weakly bound particle, which is the electron in our case. R is the distance between donor and acceptor and W_0 is the limit probability of recombination in the case of an infinitesimally close pair. Moreover, the probability of recombination can be considered as the inversion of radiative lifetime of a given DAP τ_{DAP} .

In the approximation of nearest-neighbor recombination, the luminescence decay time of one DAP will be mono-exponential. Therefore, we can assume that the luminescence intensity decay $I_R(t)$ of a single DAP pair will have form

$$I_R(t) = A \cdot \exp\left(\frac{-t}{\tau_{DAP}(R)}\right) = W(R) \exp\left(\frac{-t}{\tau_{DAP}(R)}\right) \quad [3]$$

if we substitute the amplitude A of the decay with probability of the recombination $W(R)$. To proceed further, the distribution of the donor-acceptor pair distances $G(R)$ must be known. In bulk material, theory of DAP distance distribution is well explored, for example,²⁷ but for complicated system such as InGaN/GaN QWs structure, the $G(R)$ has to be obtained numerically, as is explained below. With known $G(R)$ we can obtain the decay curve of the whole donor-acceptor system simply by summation of $I_R(t)$ for each time t

$$I(t) = \sum_R I_R(t) \cdot G(R) \quad [4]$$

Moreover, we can obtain the time-dependent energy shift from this model. Let E_R be the energy shift of a given pair caused by Coulombic interaction. In the first approximation, the interaction

between the charged ions at distance R can be described by

$$E_R = k_e \frac{e^2}{\epsilon R} \quad [5]$$

where e is the elementary charge and ϵ is the static permittivity of the material ($\epsilon_r = 10$ was assumed for GaN²⁸) and k_e is the Coulomb constant. The mean energy shift of the whole DAP system at given time t can then be estimated:

$$E(t) = \frac{\sum_R E_R \cdot I_R(t) \cdot G(R)}{\sum_R I_R(t) \cdot G(R)} \quad [6]$$

As explained above, to apply the model for the time shift of ZnB, the $G(R)$ distribution must be known. Therefore, we used the SIMS profiles of Zn and Si (assumed Si to be the donor involved in the DAP recombination) and performed numerical simulation of random distribution of Zn and Si atoms in the structure according to the depth distribution of the atoms in the InGaN QWs obtained experimentally by SIMS. The lateral dimensions were taken large enough to have at least 70 000 Zn atoms for each sample. The depth resolution of the simulation was 1 nm and the studied region involved only the 5 closer-to-substrate QWs because of the SIMS measurement artefacts as mentioned earlier. For these concentration profiles, the nearest-neighbor donor and acceptors were found, and their Euclidian distance was used. Example of histogram representing the $G(R)$ distribution probability is shown in Fig. 7 (sample P3).

Unfortunately, we do not have the SIMS data of Si for sample P1. Therefore, even Si distribution was assumed in the InGaN QWs equal to 10^{17} cm^{-3} . Calculation by Eqs. 4 and 6 and comparison with experimental results are shown in Figs. 8a–8c and 9a–9c,

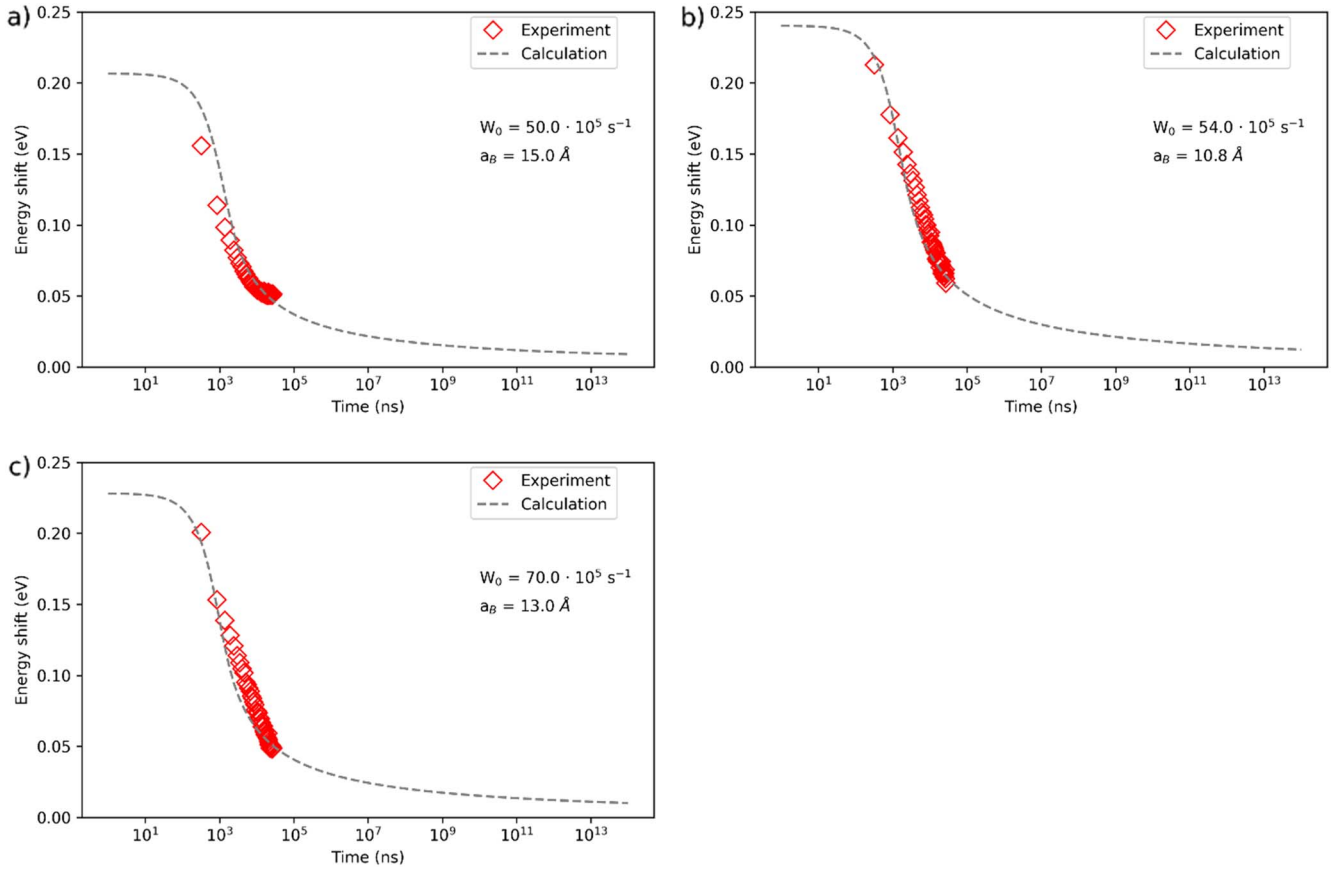


Figure 9. Energy shifts from time-resolved photoluminescence for the samples (a) P1, (b) P2, (c) P3 and the calculated profiles using Eq. 6. The parameters of the calculation are given in the picture.

Table II. Calculation parameters for samples P1, P2 and P3.

Sample	α_B (Å)	W_0 (10^5 s^{-1})	E_0 (eV)
P1	15.0	50	2.39
P2	10.8	54	2.37
P3	13.0	70	2.40

respectively. Experimental $E(t)$ were obtained from fits of the time resolved spectra (example in Fig. 6a) with the Eq. 1.

The shift measured experimentally also needs the energy E_0 representing the energy of recombination at infinite long time. Calculation parameters are given in the Fig. 9 and in Table II.

The proposed model reproduces well the experimental data for both decay curves and the energy shifts allowing to deduce the parameters W_0 and a_B summarized in Table II. The weak dispersion of the obtain values is coherent with the model. One can note a small Bohr radius for the shallow donor. In GaN, the Bohr radius for Si is calculated to be 28 Å.²² The much smaller value obtained from the calculation can be ascribed to the quantum confinement effect. The lowering of the Bohr radius in the QW and its surroundings is well documented and theoretically explained.^{29,30} In short, the electron bound to a donor in InGaN QW feels the extra confinement potential caused by GaN barriers preventing the electron movement in growth direction. The quantum confinement is also probably responsible for efficient DAP recombination at room temperature because it increases the activation energy of the donor ensuring the process

is not thermally quenched or replaced by electron-acceptor (e-A) recombination mechanism.

We should mention that the Bohr radius lowering is probably not only one-dimensional in the growth direction, but the Bohr radius might also be reduced in the lateral dimension. This would be caused by local potential fluctuations on the nm scale in InGaN alloy which are present because of the random In concentration fluctuations and well width fluctuations.^{31–33}

Time-resolved measurements clearly show that Zn impurity elimination is necessary for applications requiring the ns resolution. On the other hand, a very efficient luminescence of ZnB at low excitation intensities (Fig. 6b) might benefit the Zn doping of InGaN layers in applications requiring a high light-yield and moderate time-resolution.

Conclusions

In summary, we examined the kinetics of the Zn impurity band in InGaN/GaN heterostructures. The important characteristics of the ZnB are the large shifts of ZnB caused by DAP recombination between Si and Zn donors in InGaN/GaN quantum heterostructures in time-resolved and excitation-intensity dependent PL spectra. A model based on DAP theory has been applied and provided explanation for the experimental data well. A smaller Bohr radius for the donor was found compared to the pure GaN material which implicates the quantum confinement effect playing a role in the recombination process. Higher donor binding energy make from the DAP recombination the dominant mechanism over e-A mechanism even at room temperature in InGaN:Zn(Si). The ZnB luminescence

is slow and therefore, detrimental for applications like TOF-PET requiring fast luminescence decay.

Acknowledgments

This work was supported by the Grantová Agentura České Republiky: No. 20-05497Y and partly by the Grant Agency of the Czech Technical University in Prague by project No. SGS22/182/OHK4/3 T/14.

ORCID

František Hájek  <https://orcid.org/0000-0002-9344-4174>

References

1. A. Hospodková, M. Nikl, O. Pachterová, J. Oswald, P. Brůža, D. Pánek, B. Foltynski, E. Hulcius, A. Beitlerová, and M. Heuken, "InGaN/GaN multiple quantum well for fast scintillation application: radioluminescence and photoluminescence study." *Nanotechnology*, **25**, 455501 (2014).
2. G. Toci, L. A. Gizzi, P. Koester, F. Baffigi, L. Fulgentini, L. Labate, A. Hospodkova, V. Jary, M. Nikl, and M. Vannini, "InGaN/GaN multiple quantum well for superfast scintillation application: photoluminescence measurements of the picosecond rise time and excitation density effect." *J. Lumin.*, **208**, 119 (2019).
3. P. Lecoq, "Pushing the limits in time-of-flight PET imaging." *IEEE Trans. Radiat. Plasma Med. Sci.*, **1**, 473 (2017).
4. S. Nakamura, "High-power InGaN/AlGaIn double-heterostructure blue-light-emitting diodes." *Tech. Dig. - Int. Electron Devices Meet.*, 567 (1994).
5. J. K. Sheu, C. J. Pan, G. C. Chi, C. H. Kuo, L. W. Wu, C. H. Chen, S. J. Chang, and Y. K. Su, "White-light emission from InGaN-GaN multi-quantum-well light-emitting diodes with Si and Zn codoped active well layer." *IEEE Photonics Technol. Lett.*, **14**, 450 (2002).
6. P. G. Eliseev, V. A. Smagley, P. Perlin, P. Sartori, and M. Osinski, "Analysis of impurity-related blue emission in Zn-doped GaN/InGaN/AlGaIn double heterostructure." *Proc. SPIE - Int. Soc. Opt. Eng.*, **2693**, 97 (1996).
7. D. O. Demchenko and M. A. Reshchikov, "Blue luminescence and Zn acceptor in GaN." *phys. rev. b - condens. Matter Mater. Phys.*, **88**, 115204 (2013).
8. A. Wolos, Z. Wilamowski, M. Piersa, W. Strupinski, B. Lucznik, I. Grzegory, and S. Porowski, "Properties of metal-insulator transition and electron spin relaxation in GaN:Si." *Phys. Rev. B*, **83**, 165206 (2011).
9. P. G. Eliseev, P. Perlin, J. Furioli, P. Sartori, J. Mu, and M. Osinski, "Tunneling current and electroluminescence in InGaN: Zn, Si/AlGaIn/GaN blue light emitting diodes." *J. Electron. Mater.*, **26**, 311 (1997).
10. J. K. Sheu, T.-W. Yeh, G. Chi, and M. J. Jou, "Luminescence of the InGaN/GaN blue light-emitting diodes." *Disp. Technol. III*, **4079**, 143 (2000).
11. T. Hubáček, A. Hospodková, J. Oswald, K. Kuldová, and J. Pangrác, "Improvement of luminescence properties of GaN buffer layer for fast nitride scintillator structures." *J. Cryst. Growth*, **464**, 221 (2017).
12. C. Haller, J. F. Carlin, G. Jacopin, W. Liu, D. Martin, R. Butté, and N. Grandjean, "GaN surface as the source of non-radiative defects in InGaN/GaN quantum wells." *Appl. Phys. Lett.*, **113**, 111106 (2018).
13. T. Hubáček et al., "Advancement toward ultra-thick and bright InGaN/GaN structures with a high number of QWs." *CrystEngComm.*, **21**, 356 (2019).
14. S. Fritze, A. Dadgar, H. Witte, M. Bügler, A. Rohrbeck, J. Bläsing, A. Hoffmann, and A. Krost, "High Si and Ge n-type doping of GaN doping - limits and impact on stress." *Appl. Phys. Lett.*, **100**, 122104 (2012).
15. J. F. Muth, J. D. Brown, M. A. L. Johnson, Z. Yu, R. M. Kolbas, J. W. Cook, and J. F. Schetzina, "Absorption coefficient and refractive index of GaN, AlN and AlGaIn Alloys." *Mater. Res. Soc. Internet J. Nitride Semicond. Res.*, **4**, 502 (1999).
16. J. Mooney and P. Kambhampati, "Erratum: get the basics right: jacobian conversion of wavelength and energy scales for quantitative analysis of emission spectra." *J. Phys. Chem. Lett.*, **4**, 19 (2013).
17. M. Boulou, M. Furtado, G. Jacob, and D. Bois, "Recombination mechanisms in GaN:Zn." *J. Lumin.*, **18-19**, 767 (1979).
18. M. A. Reshchikov, "Measurement and analysis of photoluminescence in GaN." *J. Appl. Phys.*, **129**, 121101 (2021).
19. J. L. Lyons, A. Janotti, and C. G. Van De Walle, "Carbon impurities and the yellow luminescence in GaN." *Appl. Phys. Lett.*, **97**, 152108 (2010).
20. F. Zimmermann, J. Beyer, C. Röder, F. C. Beyer, E. Richter, K. Irmscher, and J. Heitmann, "Current status of carbon-related defect luminescence in GaN." *Phys. Status Solidi*, **218**, 2100235 (2021).
21. M. A. Reshchikov et al., "Two charge states of the C N acceptor in GaN: evidence from photoluminescence." *Phys. Rev. B*, **98**, 125207 (2018).
22. T. Vaněk, V. Jary, T. Hubáček, F. Hájek, K. Kuldová, Z. Gedeonová, V. Babin, Z. Remeš, and M. Buryi, "Acceleration of the yellow band luminescence in GaN layers via Si and Ge doping." *J. Alloys Compd.*, **914**, 165255 (2022).
23. T. Ogino and M. Aoki, "Mechanism of yellow luminescence in GaN." *Jpn. J. Appl. Phys.*, **19**, 2395 (1980).
24. M. A. Reshchikov, J. D. McNamara, H. Helava, A. Usikov, and Y. Makarov, "Two yellow luminescence bands in undoped GaN." *Sci. Reports*, **8**, 1 (2018).
25. O. Ambacher et al., "Pyroelectric properties of Al(In)GaIn/GaN hetero- and quantum well structures." *J. Phys. Condens. Matter*, **14**, 3399 (2002).
26. M. A. Reshchikov and H. Morkoç, "Luminescence properties of defects in GaN." *J. Appl. Phys.*, **97**, 061301 (2005).
27. H. Reiss, C. S. Fuller, and F. J. Morin, "Chemical interactions among defects in germanium and silicon." *Bell Syst. Tech. J.*, **35**, 535 (1956).
28. Y. Lei, H. Shi, H. Lu, D. Chen, R. Zhang, and Y. Zheng, "Field plate engineering for GaN-based Schottky barrier diodes." *J. Semicond.*, **34**, 054007 (2013).
29. S. Perraud, K. Kanisawa, Z.-Z. Wang, and T. Fujisawa, "Direct measurement of the binding energy and bohr radius of a single hydrogenic defect in a semiconductor quantum well." *Physical Review Letters*, **100**, 056806 (2008).
30. P. Harrison and A. Valavanis, "Impurities." *Quantum wells, wires and dots: theoretical and computational physics of semiconductor nanostructures* (Wiley, Chichester, UK) 4th ed. (2016), 10.1002/9781118923337.
31. N. K. Van Der Laak, R. A. Oliver, M. J. Kappers, and C. J. Humphreys, "Role of gross well-width fluctuations in bright, green-emitting single InGaIn/GaN quantum well structures." *Appl. Phys. Lett.*, **90**, 121911 (2007).
32. Y. S. Lin, K. J. Ma, C. Hsu, S. W. Feng, Y. C. Cheng, C. C. Liao, C. C. Yang, C. C. Chou, C. M. Lee, and J. I. Chyi, "Dependence of composition fluctuation on indium content in InGaIn/GaN multiple quantum wells." *Appl. Phys. Lett.*, **77**, 2988 (2000).
33. S. Chichibu, T. Sota, K. Wada, and S. Nakamura, "Exciton localization in InGaIn quantum well devices." *J. Vac. Sci. Technol. B Microelectron. Nanom. Struct. Process. Meas. Phenom.*, **16**, 2204 (1998).